International Journal of Multiphase Flow 134 (2021) 103469

Contents lists available at ScienceDirect

International Journal of Multiphase Flow

journal homepage: www.elsevier.com/locate/ijmulflow

Onset of water accumulation in oil/water pipe flow – experiments and modelling with LedaFlow

Jørn Kjølaas*, Marita Wolden

SINTEF, Norway

ARTICLE INFO

Article history:
Received 3 May 2020
Revised 14 August 2020
Accepted 21 September 2020
Available online 28 September 2020

ABSTRACT

In oil/water flows with very low water rates, the steady-state water fraction jumps discontinuously from a low value to a high value when the oil rate falls below the critical value. This jump is understood to be connected to the existence of multiple solutions, and generally takes place when the oil rate becomes too low to sustain a low water fraction. We refer to this critical oil flow rate as the onset of water accumulation. Water accumulation in oil transport lines is undesirable because it can lead to corrosion problems that can threaten the integrity of the installation, potentially leading to oil leaking undetected into the environment, jeopardizing nearby wildlife and ecosystems. It is therefore critical to maintain a flow rate that is high enough to prevent water from accumulating in oil lines, and the ability to predict the minimum allowable flow rate accurately is thus of great importance. To address this challenge, a new and unique set of experiments were conducted at the SINTEF Multiphase Laboratory. The experiments were specially designed to measure the critical conditions for water accumulation in oil/water flows and were performed with a pipe diameter of 8 inches (194 mm) and a pipe inclination of 2.5 degrees. The fluid system consisted of Exxsol D60 as the oil phase and regular tap water as the aqueous phase. In these experiments, the measured critical superficial water velocities were in the range 0.1-2.6 mm/s, while the critical superficial oil velocities were in the range 0.3-0.5 m/s. We found that the customary approach of modelling the oil/water interfacial shear stress as a smooth wall was inadequate for predicting these experiments, and that interfacial waves must be considered. The data analysis showed that the onset of interfacial waves is well predicted by Viscous Kelvin-Helmholtz theory, and that a model for the interfacial shear stress can be constructed with this theory as a starting point. A new model for oil/water interfacial shear stress was developed based on this data and the associated data analysis. The new model was able to match the experimental data well and a slightly modified version of it was ultimately implemented in the commercial multiphase flow simulator LedaFlow.

1. Introduction

Because of the increasing awareness and concern about the impact of fossil fuels on climate change, as well as the depletion of current oil reserves, oil production is expected to decline substantially in the coming years. Although this trend is desirable from an environmental perspective, it will have negative consequences for oil transport lines which have typically been designed for high throughput. One of the problems that will occur is that the decline in the flow velocity allows small amounts of water in the system oil (due to imperfect separation) to segregate out during transport and to accumulate in the inclined parts of the line. Specifically, if the flow velocity becomes sufficiently low, the water can separate and accumulate in uphill regions, creating pools of water that are essentially stagnant, see Fig. 1. This is a highly undesirable situation because free water can lead to corrosion problems on the inside of the pipe which can ultimately lead to oil leaking undetected into the surroundings, contaminating the environment (Magill, 2012). An example where such problems are expected to occur is the Trans Alaska Pipeline System, which transports oil 800 miles from the North Slope oil fields south to Valdez on Prince William Sound (Trans Alaska Pipeline System - The facts, 2019). For that system the ambient temperature is typically sub-zero, and the near-stagnant water can eventually freeze, yielding an even more hospitable environment for corrosion. In that scenario, chunks of ice could also periodically be pushed through the line and possibly cause damage to pump station equipment (Bluemink, 2010).

* Corresponding author.
E-mail address: jorn.kjolaas@sintef.no (J. Kjølaas).

https://doi.org/10.1016/j.ijmultiphaseflow.2020.103469

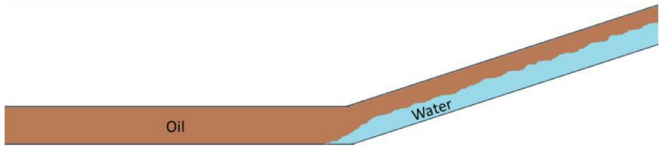

Fig. 1. Illustration of water accumulation in uphill pipe sections.

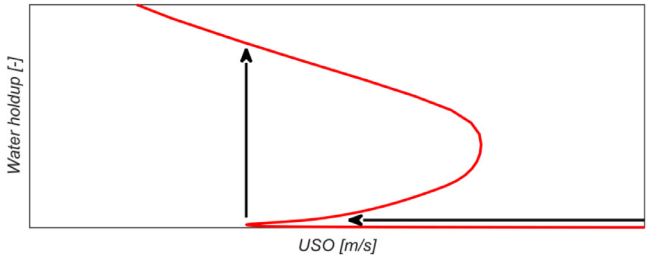

Fig. 2. Example of the multiple solutions region in oil/water flows, where multiple water fractions are valid solutions to the steady-state equations for a range of superficial oil velocities *USO*.

Efficient mitigation procedures require knowledge about where and how fast the water can accumulate, and accurate models are then needed to make such assessments. Indeed, all preventive measures come at cost, and could threaten the economic viability of the pipeline if they become too high. By having predictive models that can forecast these problems, one can obtain a more accurate picture of the required expenditures.

The primary physical mechanism that determines whether water will accumulate is the interfacial shear stress between oil and water. When the oil rate is low, the water will settle at the bottom of the pipe but will continue to flow as a thin film if the interfacial shear stress is sufficiently high. From a practical perspective, this situation is arguably acceptable because the exposure to corrosion problems are then minimal. However, if the oil rate drops below some critical value, the water will almost stop moving and it will instead accumulate (see Fig. 1). This transition can be very distinct, and at sufficiently low water rates, the transition is completely discontinuous. We refer to this discontinuous jump as "the onset of water accumulation", and in this paper we will present experiments that explore this phenomenon.

From a modelling perspective, this phenomenon can be explained by the notion that the steady-state flow equations have more than one solution in a certain range of oil flow rates (Barnea and Taitel, 1992) (Landman, 1991) (Ullmann et al., 2003), see Fig. 2. In the multiple solution region, there are three hypothetical solutions, and the system will then in most circumstances "select" the one with the lowest water holdup (Kjølaas and Holm, 2016). However, below a certain oil flow rate, the low-holdup-solution ceases to exist, and then the system has no choice than to approach the high-holdup-solution. If the oil rate drops below this point, the water will accumulate until the high-holdup-solution is obtained. We will discuss this matter in more detail in the modelling part of this paper.

In the scientific literature, we have found no articles addressing the challenge of predicting water accumulation in oil/water flows. Even the modelling of interfacial shear stress between oil/water in general seems to be universally neglected in the literature, as virtually all authors (Brauner et al., 1998) (Hall and Hewitt, 1993) (Valle and Kvandal, 1995) resort to assuming a smooth oil/water interface, disregarding the effect of interfacial waves. Taitel et al. (1995) and Valle (2000), deviated slightly from this basic approach by introducing a lower limit of 0.014 on the interfacial friction factor. Zaghloul et al. (2008) simply elected to use a constant value of 0.014. Our data analysis will however show that this simplified approach is inadequate for predicting water accumulation in inclined pipes, because the effect of interfacial waves leads to significantly elevated values of interfacial shear stress.

In Section 3 of this paper we present a set of new and unique large-scale oil/water experiments that were specially designed to identify the onset of water accumulation for different flow conditions. In these experiments we use a special technique that is essentially the same as the one used previously for gas-liquid flows (Kjølaas et al., 2015).

In Section 4 of this paper we address the modelling of the interfacial shear stress between oil and water, focusing on the prediction of water accumulation in oil/water flows as the main application. It should however be emphasized that the oil/water interfacial friction factor is a model that can be used in all scenarios where oil and water flow as separate phases and can therefore be important in many other circumstances.

2. The LedaFlow 1D model

In this paper, we have elected to use the 1D multiphase flow simulator "LedaFlow" ("LedaFlow, " Kongsberg Digital AS, 2020) as a framework for simulating the new oil/water experiments, and for addressing the modelling of water accumulation in oil/water flows. In this section we provide a brief non-exhaustive description of the what this software does, and what equations it solves.

2.1. Conservation equations

LedaFlow is a transient three-phase flow simulator designed to simulate multiphase flow in pipes. The transport equations are solved in one dimension along the flow direction. The flow is generally represented by nine fields: continuous gas, oil and water, plus all possible dispersed fields, see Fig. 3.

The 1D mass conservation equations are solved for each of the nine fields k:

$$\frac{\partial (A\alpha_k\rho_k)}{\partial t} + \frac{\partial}{\partial x}(A\alpha_k\rho_k u_k) = A\sum_{i\neq k}\Gamma_{k,i} + A\Gamma_{k,ext} \tag{1}$$

Here, A is the cross section pipe area, and α_k, ρ_k and u_k are the volume fraction, density and velocity of field k. $\Gamma_{k,i}$ represents mass transfer terms due to condensation/evaporation, and $\Gamma_{k,ext}$ represents external mass sources.

Each continuous field combined with its two constituent dispersed fields is defined as a "zone". For each zone, the associated momentum equation is solved in the flow direction. In the experiments presented in this paper, the oil and water flow as separate phases with negligible oil/water entrainment because of the low velocities. This makes the modelling more straightforward by allowing us to ignore the dispersed fields in our analysis. Indeed, for the special case of oil/water flow with no mass transfer and no dispersed fields, the momentum equations reduce to:

$$\begin{aligned}&\tfrac{\partial}{\partial t}(A\alpha_o\rho_o u_o) + \tfrac{\partial}{\partial x}\left(A\alpha_o\rho_o u_o^2\right) = -A\alpha_o\tfrac{\partial p}{\partial x}\\ &-A\alpha_o\rho_o g_x - A\alpha_o g_y(\rho_o-\rho_g)\tfrac{\partial h_o}{\partial x} - S_o\tau_o - S_{ow}\tau_{ow}\end{aligned} \tag{2}$$

$$\begin{aligned}&\tfrac{\partial}{\partial t}(A\alpha_w\rho_w u_w) + \tfrac{\partial}{\partial x}\left(A\alpha_w\rho_w u_w^2\right) = -A\alpha_w\tfrac{\partial p}{\partial x}\\ &-A\alpha_w\rho_w g_x - A\alpha_w g_y\left[(\rho_o-\rho_g)\tfrac{\partial h_o}{\partial x} + (\rho_w-\rho_o)\tfrac{\partial h_w}{\partial x}\right]\\ &-S_w\tau_w + S_{ow}\tau_{ow}\end{aligned} \tag{3}$$

Here, the indices o and w refer to "oil" and "water", p is the pressure, g_x is the acceleration of gravity in the flow direction, g_y is the acceleration of gravity normal to the flow, h_o and h_w are the respective heights of the oil/water layers, S_o and S_w are the oil/water wall perimeters, S_{ow} is the oil/water interface length, τ_o and τ_w are the oil/water wall shear stresses, and τ_{ow} is the interfacial shear stress between the oil and the water. For near-horizontal

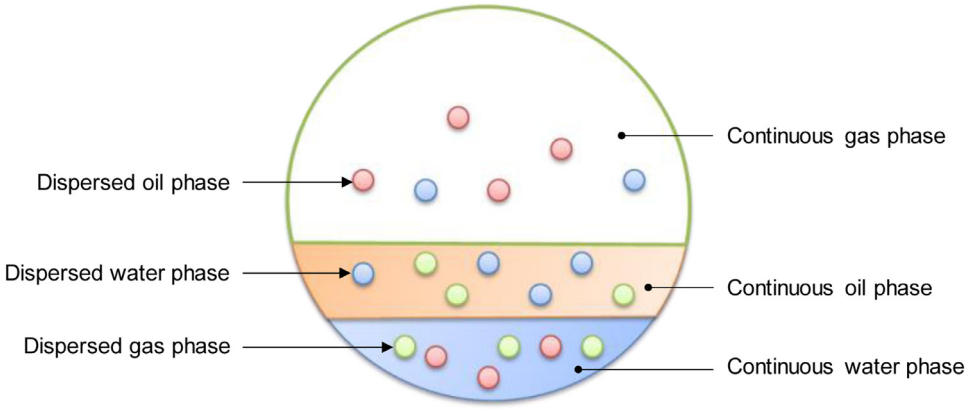

Fig. 3. Continuous and dispersed fields in LedaFlow.

flows, the geometrical parameters S_o, S_w and, S_{ow} are calculated assuming a flat oil/water interface.

In steady-state fully developed flow, the momentum equations can be simplified further by removing the temporal and spatial derivatives, except for the pressure derivative (which for obvious reasons cannot be neglected):

$$0 = -A\alpha_o \frac{\partial p}{\partial x} - A\alpha_o \rho_o g_x - S_o \tau_o - S_{ow}\tau_{ow} \tag{4}$$

$$0 = -A\alpha_w \frac{\partial p}{\partial x} - A\alpha_w \rho_w g_x - S_w \tau_w + S_{ow}\tau_{ow} \tag{5}$$

The analyses presented in this paper will primarily be based on Eqs. (4) and (5), as the prerequisites for using these equations are generally fulfilled in our experiments.

2.2. Closure relations

The shear stress terms τ_o, τ_w and τ_{ow} are modelled using a certain set of closure relations in LedaFlow, but we will not describe those in detail here. Instead, we have for the purpose of this analysis replaced the usual LedaFlow closure laws with "standard" closure laws from the literature, and we have thus used LedaFlow only as a vehicle for solving the 1D transport equations. We found that our results did not depend critically on the choice of closure laws, so we have chosen to use quite simple formulations:

The wall shear stress for zone k is in LedaFlow expressed as:

$$\tau_k = \frac{1}{2} f_k \rho_k |u_k| u_k \tag{6}$$

We have in this paper elected to calculate the friction factor f_k in Eq. (6) as:

$$f_k = f_{k,lam}^{W} \cdot f_{k,turb}^{1-W} \tag{7}$$

Here, $f_{k,lam}$ is the friction factor for laminar flow:

$$f_{k,lam} = \frac{16}{\mathrm{Re}_k} \tag{8}$$

and $f_{k,turb}$ is the friction factor for turbulent flow, where we use the expression proposed by Håland (1983):

$$\frac{1}{\sqrt{f_{k,turb}}} = -3.6 \cdot \log_{10}\left[\frac{6.9}{\mathrm{Re}_k} + \left(\frac{\varepsilon}{3.7 D_{hk}}\right)\right]^{1.11} \tag{9}$$

Here, Re_k is the Reynolds number which we define as:

$$\mathrm{Re}_k = \frac{\rho_k u_k D_{hk}}{\mu_k} \tag{10}$$

Table 1
Fluid properties.

Property	**Value**
Oil density [kg/m3]	795
Water density [kg/m3]	999
Oil viscosity [cP]	1.5
Water viscosity [cP]	1
Oil/water surface tension [mN/m]	19

where μ_k is the phase viscosity and D_{hk} is the hydraulic diameter which we define as:

$$D_{hk} = \frac{4\alpha_k A}{S_k} \tag{11}$$

Finally, the laminar/turbulent weighting function W is defined as:

$$W = \frac{1}{1 + \left(\frac{\mathrm{Re}_k}{2300}\right)^{20}} \tag{12}$$

The starting point for this work is to model the interfacial shear stress as a smooth wall using the expression described by Eq. (20) later in this paper. The purpose of this work is however to find a more appropriate expression for the interfacial shear stress than the smooth wall assumption.

3. Experiments

In this section we describe the flow loop setups and procedures used to conduct the experiments.

3.1. Experimental setup

The experiments were conducted in a 94 m long 8" pipe (inner diameter 194 mm) with a 2.5° inclination using Exxsol D60 as the oil phase and tap water as the aqueous phase. The setup is illustrated in Fig. 4. The pipe was equipped with six pressure-transmitters (labelled P) that were coupled to a common gas-filled reference line, six vertically mounted narrow-beam gamma densitometers to measure local water heights (labelled γ), and two traversing gamma densitometers (labelled $T\gamma$ in Fig. 4). Finally, temperature transmitters (labelled T) were mounted at the beginning and end of the test section. The thermodynamic properties of the fluids are listed in Table 1.

3.2. Outlet

The end of the 8" inclined pipe expands into a short 12" pipe with the same inclination, followed by an 80 cm long 12" horizon-

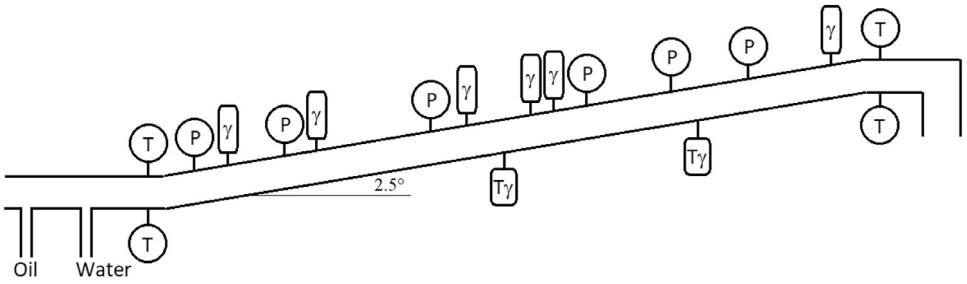

Fig. 4. Schematic illustration of the test section used in the experiments.

tal pipe, a 90 degree downward bend and a vertical 12" downward pipe. Initially we had some concerns about the design of this outlet, fearing that water might accumulate in the 12" inclined pipe, which could perceivably influence the flow in the 8" test section. Specifically, any water that accumulated there could flow back into the 8" pipe and increase the water content.

However, transient simulations of the experiments using LedaFlow ("LedaFlow, " Kongsberg Digital AS, 2020) showed that gas would always be present at the top of the 12" pipe, so that the available area for the liquid actually decreased in the 12" pipe, yielding increased flow velocities instead of decreased velocities. Based on this analysis, there was thus no real danger of water accumulating there, and the pipe expansion was ultimately not considered a problem. Also, had this actually been a problem, we would have readily noticed it during the experiments.

3.3. Gamma densitometers

All the gamma densitometers consisted of a Caesium radiation source on one side of the pipe and a photon detector on the other side. The attenuation of the photon beam decreases exponentially with the density of the medium between the source and detector, allowing us to measure the average density along the rays' travel path. By recording the photon count rates with pure oil and pure water in the pipe, the measured photon rates in oil/water experiments could be converted to water fractions, which is what we show in this paper.

The gamma densitometers were collimated on both the source side and the detector side. With this type of arrangement, scattered photons rarely reach the detector, and the prevailing accuracy has been shown to be about 0.02 for oil-water systems. All gamma densitometers were logged at 50 Hz, and the traversing instruments scanned the pipe from bottom to top with a constant velocity of 0.4 mm/s.

Example results from a traversing gamma densitometer (top graph) and a vertically mounted static gamma densitometer are shown in Fig. 5 (bottom graph). The traversing gamma densitometer gives the time-averaged water fraction profile, while the static gamma densitometer gives the instantaneous water height. We observe that the oil and water flow as separate phases, with significant waves on the surface (the diffuse interface observed with the traversing gamma is caused by waves). The total water fraction was obtained by integrating the water fraction profiles over the pipe cross section.

3.4. Steady-state experiments

Steady state experiments are experiments designed to obtain the phase fractions and pressure drop at steady (non-transient) conditions. These types of experiments are the most common ones for studying multiphase flows. At the low flow rates examined in this paper, flow transients can be very slow, and it was therefore very important to allow the flow to stabilize for sufficiently long

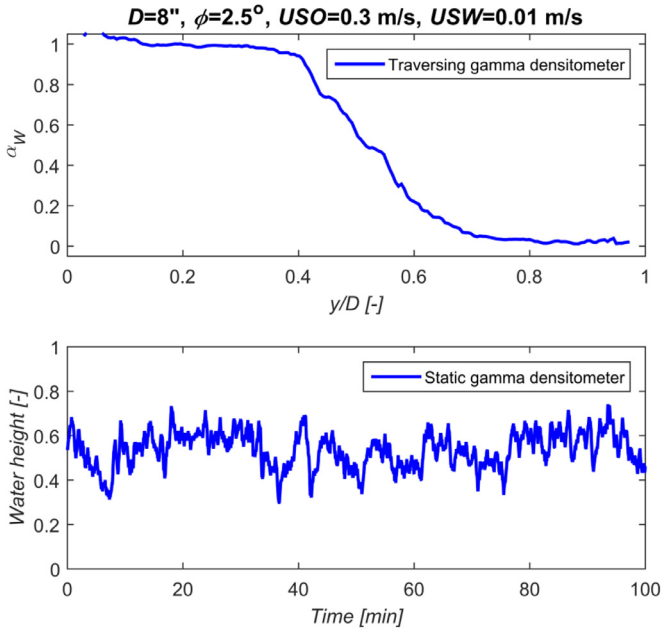

Fig. 5. Example results from a traversing gamma densitometer (top graph) and a vertically mounted static gamma densitometer (bottom graph).

before recording the experiments. The stabilization times between experiments were typically around 20-30 minutes.

3.5. Screening experiments

In previous publications (Kjølaas and Holm, 2016) (Kjølaas et al., 2015), we have used the term "screening experiments" for experiments designed to find the discontinuous transition between high and low holdup in low liquid loading flows. Although this term is arguably not a very descriptive one, we continue to use it here for consistency. In this paper we use the term in the context of oil/water flows (as opposed to gas-liquid flows). In other words, the experiments described here are essentially equivalent to those presented in Kjølaas et al. (2015), except that the gas/liquid system has been replaced by oil/water, and the current objective was to find the discontinuous transition between high and low water fraction for low water rates.

As mentioned in the introduction, the discontinuous transition between low/high water holdup is closely connected to the existence of multiple holdup solutions, i.e. that more than one flow configuration is in principle possible for a set of boundary conditions. We discuss this in more detail in Section 3.7.

The main principle of this experiment technique is that we perform measurements in a quasi-steady-state situation, with a high water holdup in the first part of the pipe, and a low holdup further downstream (see Fig. 6). Here we are in practice in a transient sit-

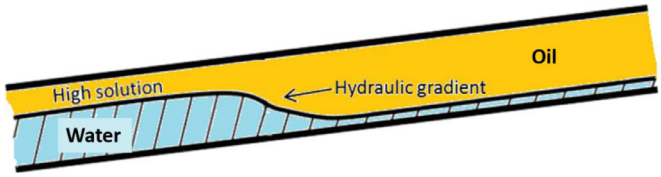

Fig. 6. Illustration of a screening experiment in two-phase oil/water flow.

uation, where the flow is transforming from a high water holdup to a low water holdup, or vice versa, depending on the overall water mass balance in the pipe. The key aspect of this experiment is that we measure the superficial water velocity out of the pipe (USW_{OUT}).

The reasoning behind this experiment technique is based on the observation that USW_{OUT} is decoupled from USW_{IN} in this situation (USW_{IN} being the superficial water velocity at the inlet). That implies that we can adjust USW_{IN} to match USW_{OUT}, so that the water front in the pipe becomes stationary. Starting from this scenario, any small increase in USW_{IN} will cause the liquid front to move towards the outlet, eventually giving a high solution in the entire pipe. Conversely, a small decrease in USW_{IN} would cause the liquid front to move towards the inlet, giving a low solution in the entire pipe. Based on this reasoning we can conclude that the critical USO/USW pair given by USO and USW_{OUT} defines the "tipping point" where the flow goes from a high holdup solution to a low holdup solution.

Building on these considerations, the following procedure was used to measure the onset of the water accumulation in two-phase flow:

- We started with an oil-filled pipe and set USO to a constant value.
- We injected water at a relatively high rate ($USW \approx 0.02$ m/s), so that the water built up at the inlet, and a water front (hydraulic gradient) propagated towards the outlet. When the water front was around the middle of the pipe, we stopped the water injection.
- We then waited until the water rate out of the pipe was steady, in order to obtain a suitable time sequence for calculating the average value of the net water flow rate in/out of the pipe. We will explain how we calculated the water flow rate out of the pipe in Section 3.6.
- The measured outlet water flow rate (USW_{OUT}) combined with the current USO was subsequently interpreted as a "critical" USO/USW pair, where the flow transforms discontinuously from a high holdup to a low holdup.
- Next, USO was ramped up to a new value, and a new value for USW_{OUT} was obtained, and so on.

If the oil rate had been ramped up to the point where only one solution was possible (with a low water fraction), the excess water would presumably have been pushed out from the inlet. We did not try this in these tests, but earlier experiments with gas/liquid have shown this to happen (Kjølaas et al., 2015). The reason this happens is that the high-holdup solution is no longer a valid solution at those conditions, and it is thus impossible to maintain a stable water front as we do in these screening experiments.

3.6. Calculation of the outlet water rate

In the current experiments we did not have a designated system for measuring the outlet water rate USW_{OUT}, so we had to come up with an alternative method for obtaining this parameter from the available instrumentation. We found that a good approach was to use the available pressure measurements:

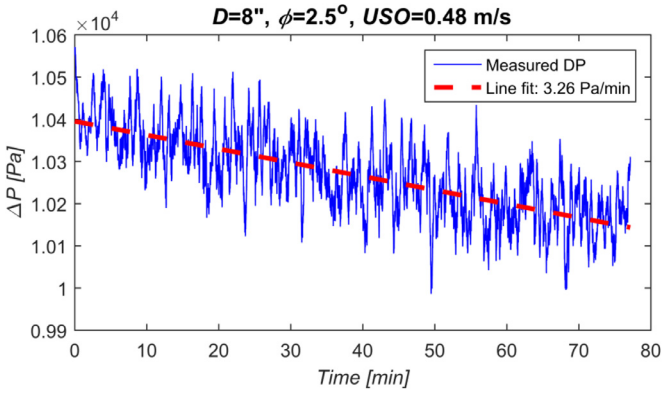

Fig. 7. Pressure difference over the water front plotted versus time for a selected experiment.

We define the water volume V_w as the total amount of water between the first and last pressure transmitter on the test section, and we define the distance between these pressure transmitters as Δx. The associated volume balance can be written as:

$$\frac{dV_w}{dt} = A\Delta x\frac{d\alpha_w}{dt} = A(USW_{IN} - USW_{OUT}) \tag{13}$$

where A is the cross-sectional area of the pipe, α_w is the average water fraction between the pressure transmitters, and USW_{IN}/USW_{OUT} are the superficial water velocities in/out of the volume V_w. Note that in the experiments in question, the water front illustrated in Fig. 6 was always somewhere between these pressure transmitters. Rearranging Eq. (13), we obtain:

$$USW_{OUT} = USW_{IN} - \Delta x\frac{d\alpha_w}{dt} \tag{14}$$

The pressure difference ΔP that we measure can be safely assumed to be dominated by gravity because of the low flow rates. This pressure difference is then given by:

$$\Delta P \approx [\alpha_w\rho_w + (1-\alpha_w)\rho_o]g\sin\phi \cdot \Delta x \tag{15}$$

Here, ρ_o and ρ_w are the oil and water densities, g is the gravity acceleration, and ϕ is the pipe angle. By differentiating Eq. (15) with respect to time, we get:

$$\frac{d\Delta P}{dt} \approx \Delta\rho g\sin\phi \cdot \Delta x\frac{d\alpha_w}{dt} \tag{16}$$

A slight rearrangement of Eq. (16) yields:

$$\Delta x\frac{d\alpha_w}{dt} \approx \frac{1}{\Delta\rho g\sin\phi}\cdot\frac{d\Delta P}{dt} \tag{17}$$

Finally, we substitute Eq. (17) into Eq. (14), yielding:

$$USW_{OUT} = USW_{IN} - \frac{1}{\Delta\rho g\sin\phi}\cdot\frac{d\Delta P}{dt} \tag{18}$$

In other words, we can estimate the water rate out of the pipe by measuring the rate at which the pressure difference across the water front varies in time. Fig. 7 shows an example of how the pressure difference decreases over time. The process is very slow, so these measurements must be conducted over relatively long time scales to obtain accurate results (typically 1-2 hours).

3.7. Interpretation of the screening experiments

We will in this section describe our interpretation and understanding of the screening experiments, and how they relate to steady-state point model predictions.

The bottom graph of Fig. 8 shows an example of a transient simulation of a screening simulation with LedaFlow ("LedaFlow, "

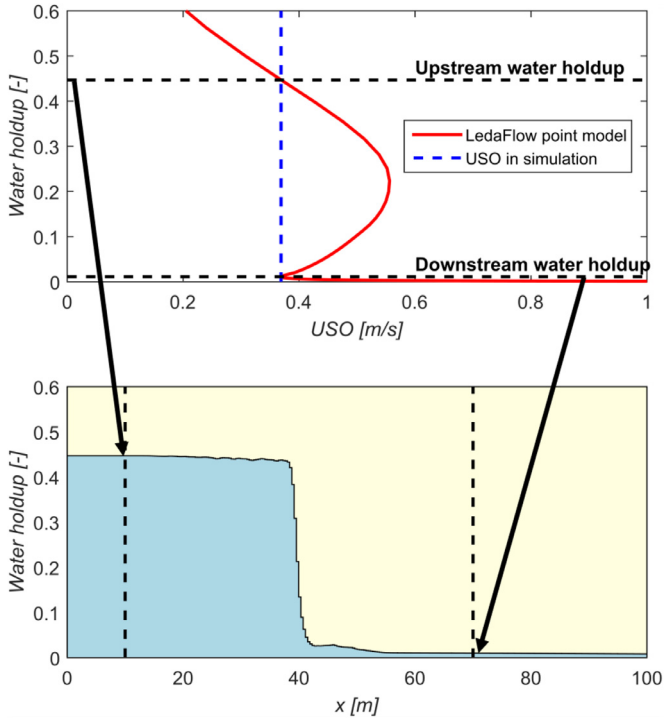

Fig. 8. Example of LedaFlow simulation results. The top plot shows the water holdup (red line) plotted against *USO* (all solutions) for USW=0.46 mm/s as predicted by the LedaFlow point model. The bottom plot shows a time-averaged picture of a screening simulation where *USO*=0.37 m/s and *USW*=0.46 mm/s.

Kongsberg Digital AS, 2020), with *USO* equal to 0.37 m/s. The transient simulation is conducted in qualitatively the same way as the experiment, where a water front has been established in the pipe. The plot shows the predicted time-averaged water fraction profile after the water front has been established.

In this simulation, the water rate at the outlet was found to be USW_{OUT}=0.46 mm/s. When adjusting the inlet water rate to match USW_{OUT}, the oil/water front in the pipe was observed to remain stationary, as expected. We may thus conclude that for this simulated case, the critical *USO* (USO_C) is 0.37 m/s when *USW*=0.46 mm/s.

The red curve in the top graph shows steady-state simulation results obtained by solving the steady-state flow equations described in Section 2.1. The conditions assumed here were the same as in the transient simulation, and *USW* was set exactly equal to the recorded outlet rate (*USW*=0.46 mm/s).

We observe here that the steady-state equations have three possible solutions in a certain range of *USOs*. The blue vertical line indicates the value of *USO* that was applied in the transient simulation (0.37 m/s), which is the critical *USO* where the water holdup switches between a high and low value. This blue line intersects the red curve at the very start of the multiple solution region, indicating that the transition between low/high water holdup occurs at the start of the multiple solution region, i.e. that the low solution is "preferred".

The two black lines in the top graph of Fig. 8 indicate the water holdups found before and after the water front in the transient simulation (the location where these values were taken is indicated by the black lines in the bottom plot). These black lines intersect the red curve in the same place as the blue line, showing that the water holdup upstream of the liquid front corresponds to the high holdup solution, while the water holdup downstream of the water front represents the low solution (at the accumulation point).

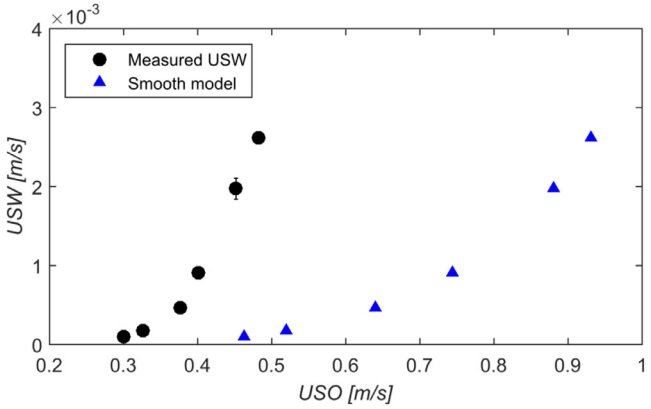

Fig. 9. Experimental and simulated outlet water rate plotted against *USO* for the screening experiments.

These results are consistent with our current understanding of how multiple solutions work, i.e. that the transition between low and high holdup occurs at the start of the multiple holdup solution region. Many dynamic simulations have been carried out using LedaFlow to confirm this matter, changing the flow rates and examining which holdup solution prevails. The results from these simulations have turned out to always be the same, namely that the transition between the high/low holdup solution occurs at that exact location.

Our understanding is that the reason for this "low-holdup-preference" has to do with the outlet boundary condition. Specifically, if the geometrical configuration of the outlet allows the water to flow out, yielding a low water holdup at the outlet, the low-holdup-solution will prevail. This has to do with the so-called level gradient forces (the *dh/dx*-terms in Eqs. (2) and (3)), which try to make the interfaces horizontal, yielding a force on the water zone in the flow direction.

We have also simulated scenarios where the test section is followed by a pipe with an even higher inclination. In this situation we have found that the water holdup solution in the first pipe depends on the water holdup in the second pipe. Specifically, if the water holdup in the second pipe is high, the water holdup in the first pipe also remains high if such a solution is possible. The reason this happens is presumably that the level gradient force on the water at the junction now points in the opposite direction, and that water is not allowed to drain naturally from the first pipe. This "low-holdup-preference" is thus not a general trait of multiple solution scenarios, but rather a consequence of the outlet boundary condition, which in most circumstances will facilitate a low water holdup.

We may add that the low-solution preference is supported experimentally by Johansson et al. (2013), where the authors went to great lengths to uncover hysteresis in these circumstances, but no hysteresis was ever found.

3.8. Experimental results

Fig. 9 shows the results obtained in the experiments, where we have plotted the outlet water rate versus the oil flow rate. The black markers are the experimental data, while the blue dashed lines are predictions made using the smooth interface model. The interpretation of these results is that water accumulates in the region to the left of these curves, while the low-holdup-solution prevails on the right-hand side. It is quite clear from these results that modelling the interface as a smooth wall yields overly "pessimistic" results.

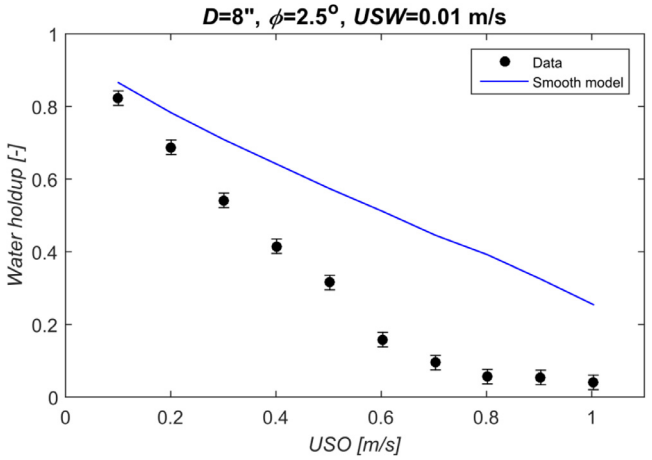

Fig. 10. Experimental and simulated water fraction plotted against *USO* for the steady-state experiments.

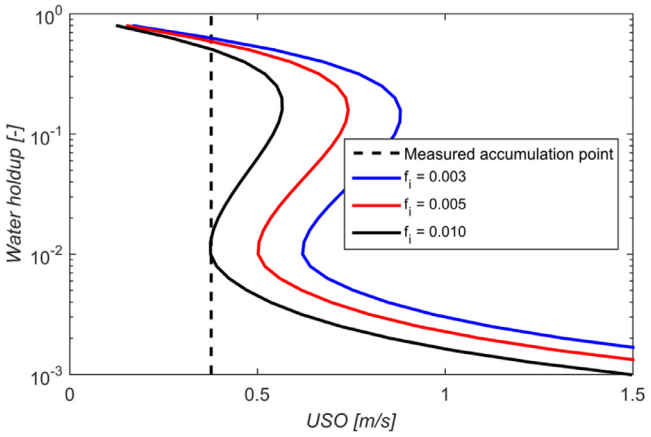

Fig. 11. Illustration of the procedure for calculating the interfacial friction factor from screening experiments.

Fig. 10 shows the results from steady-state experiments, where the superficial oil velocity *USO* was varies from 0.1 to 1.0 m/s, while superficial water velocity *USW* was fixed to 0.01 m/s. We observe that the "smooth model" severely over-predicts the water holdup, indicating that the interfacial shear stress is too small.

4. Data analysis and modelling

In this section we analyse the experimental data presented in the previous section to obtain values of the interfacial friction factor for the different cases, and we subsequently use those values to derive a new model for the oil/water interfacial shear stress.

4.1. Calculating the interfacial friction factor from steady-state experiments

The standard method for calculating the interfacial friction factor f_i from steady-state multiphase experiments is to insert a mixture of measured quantities and closure relationships into the steady-state momentum equations, and back out the interfacial shear stress. There are several possible ways of doing this, but the approach that we used in this paper was to combine the oil/water momentum Eqs. (4) and ((5)) and eliminate the pressure gradient. Re-arranging the terms of the prevailing equation yields the following expression:

$$\tau_{ow} = \frac{A(\rho_w - \rho_o)g_x + \frac{S_w}{\alpha_w}\tau_w - \frac{S_o}{\alpha_o}\tau_o}{\frac{S_{ow}}{\alpha_w} + \frac{S_{ow}}{\alpha_o}} \tag{19}$$

By inserting the closure laws summarized in Section 2.2, the interfacial shear stress τ_{ow} was backed out, and the interfacial friction factor could subsequently be calculated using Eq. (23).

The main weakness of this approach is that the results depend a great deal on the validity of the closure laws that we have supposed, as well as the accuracy of the phase fraction measurements. The latter issue is especially a problem when one of the phase fractions is small, because the measurement error for the small phase fraction can then yield very high relative uncertainties in the friction factor estimates.

Because of these weaknesses, this approach is not the primary one used in this paper. Instead we mainly base the modelling on the approach outlined in the next section. Also, it should be mentioned that several of the steady-state experiments were excluded from this analysis on the grounds that the prevailing uncertainties in the friction factor estimates were so large that the friction factor values were arguably not meaningful.

4.2. Calculating the interfacial friction factor from screening experiments

The uncertainty problems listed in the previous section are largely mitigated with the approach that we utilize here, which is identical to the method used in Kjølaas and Holm (2016). In simple terms, the procedure that we use to calculate the oil/water interfacial friction factor is to "guess" the value of the interfacial friction factor until the predicted water accumulation point (the start of the multiple holdup solution region) matches the measured value. Fig. 11 illustrates how this works. Here we plotted water holdup curves with all solutions for a certain water flow rate (which was measured in the experiment), using different values of the interfacial friction factor. The vertical dashed line represents the measured superficial oil velocity. The procedure is simply to find the value of f_i that makes the model match the measured accumulation point. In the example provided in Fig. 11, the black line (f_i =0.01) gives the best match.

It should be noted that this interfacial friction factor only applies to the low-holdup solution, and not to the high-holdup solution. The reason for this is that the water flow rate out of the pipe in the screening experiments are exclusively determined by the force balance on the liquid film downstream of the gas/liquid front. Consequently, it is the oil's ability to pull this water film that we have measured, and the flow in the high-water-holdup region is decoupled from this.

We must also mention that in this analysis, we have in principle assumed that the selected closure laws for the wall shear stresses are correct. This is however of minor concern, as the results have been found to be only weakly coupled to the wall shear stresses.

It is also worth noting that in the experiments addressed in this paper, there is essentially no droplet entrainment, meaning that the experimental results can be assumed to be a sole product of friction and gravity forces. If there was significant entrainment in these experiments, the associated momentum transfer would have to be accounted for in the analysis, which would be an exceedingly difficult task.

4.3. Smooth oil/water flow

The underlying idea behind modelling interfacial shear stress is that the interface can be viewed as a moving wall from the perspective of the phases on each side of the interface. Specifically, if the interface is smooth, i.e. with no interfacial waves, it can be modelled as a smooth wall. On the other hand, if there are waves on the interface, those waves will tend to increase the interfacial

friction coefficient for the same reason as a rough wall will increase the wall friction. In LedaFlow, we use the following expression for the interfacial friction coefficient $f_{i,smooth}$ for smooth interfaces:

$$f_{i,smooth} = \frac{\rho_{ow} f(Re_o) f(Re_w)}{\left[\sqrt{\rho_o f(Re_o)} + \sqrt{\rho_w f(Re_w)}\right]^2} \tag{20}$$

Here, the interface density ρ_{ow} is defined as:

$$\rho_{ow} = \sqrt{\rho_o \rho_w} \tag{21}$$

Here, Re_o and Re_w are the Reynolds numbers for oil and water, and $f(Re_o)$ and $f(Re_w)$ are smooth wall friction factors obtained from the wall friction model described by Eq. (7), based on oil- and water zone properties and the respective velocities relative to the interface (u_o-u_i and u_w-u_i), where the interface velocity u_i is defined as:

$$u_i = \frac{\sqrt{\rho_o f(Re_o)} u_o + \sqrt{\rho_w f(Re_w)} u_w}{\sqrt{\rho_o f(Re_o)} + \sqrt{\rho_w f(Re_w)}} \tag{22}$$

Finally, the interfacial shear stress τ_i is expressed as:

$$\tau_i = \frac{1}{2} f_i \rho_{ow} |u_o - u_w| (u_o - u_w) \tag{23}$$

In the case of a smooth interface, the interfacial friction coefficient f_i takes on the value of $f_{i,smooth}$, while if there are waves on the interface, a higher value is expected.

A key aspect of this formulation is that it is symmetrical with respect to the oil/water phases, so that interchanging the oil and water properties leads to the same expression.

4.4. The onset of oil/water waves

The primary challenge with modelling the interfacial shear stress is to incorporate the effect of interfacial waves on the interfacial friction factor. Here, the first question that we must address is:

Under what conditions does the interface go from smooth to wavy?

To answer this question, we turn to Viscous Kelvin-Helmholtz (VKH) analyses, which is the study of wave growth. In the present analysis, we use the expression derived by Funada & Joseph (Funada and Joseph, 2001), who included the effect of surface tension and viscosity on the normal stress, while neglecting the effects of the shear stresses. Using these assumptions, they showed that the onset of waves with a dimensionless wave number k (made dimensionless using the pipe diameter D) occurs when the slip velocity Δu exceeds u_c, given by:

$$u_c^2 = \frac{\left[\tanh(k\cdot\alpha_o) + \frac{\mu_o}{\mu_w}\tanh(k\cdot\alpha_w)\right]^2}{\tanh(k\cdot\alpha_o) + \left(\frac{\mu_o}{\mu_w}\right)^2 \frac{\rho_w}{\rho_o}\tanh(k\cdot\alpha_w)} \frac{1}{k}\left(1 + \frac{k^2}{Eo}\right) \cdot \frac{\Delta\rho \cdot g}{\rho_o} \cdot \frac{dh_w}{d\alpha_w} \tag{24}$$

Here, μ_o and μ_w are the oil/water viscosities, Eo is the Eötvös number ($Eo = \Delta\rho g D^2/\sigma_{ow}$) and h_w is the water height. It should be noted that the original expression provided by Funada & Joseph was derived for channel flow and is slightly different from Eq. (24) which has been adapted to pipe flow.

In order to deduce the onset of waves from Eq. (24), we must select a certain (dimensionless) wave number k. The logical choice here is to select the wave number that gives the lowest value for u_c, since the first waves that will grow on the interface will have that wave number. Fig. 12 shows an example of how the wave onset velocity u_c typically depends on the wave number.

We observe that u_c has a minimum, and we can say that the wave number at that minimum represents the "most dangerous" wave. It is possible to determine this critical wave number k_c by solving the equation $du_c/dk=0$, but unfortunately, this equation does not have an analytical solution. We could alternatively elect to solve this equation numerically, but we have found that the critical wave number can be approximated well by first assuming that k is large compared to the volume fractions. For large k, the *tanh*-terms in Eq. (24) can be replaced by unity, and it is then a straightforward exercise to show that the critical wave number k_c is given by:

$$k_c^2 \approx Eo = \frac{\Delta\rho g D^2}{\sigma_{ow}} \tag{25}$$

Here, D is the pipe diameter and σ_{ow} is the oil/water surface tension. The wave onset velocity u_c can then be found by substituting the dimensionless wave number k in Eq. (24) by the wave number given by Eq. (25):

$$u_c^2 = \frac{\left[\tanh(k_c\cdot\alpha_o) + \frac{\mu_o}{\mu_w}\tanh(k_c\cdot\alpha_w)\right]^2}{\tanh(k_c\cdot\alpha_o) + \left(\frac{\mu_o}{\mu_w}\right)^2 \frac{\rho_w}{\rho_o}\tanh(k_c\cdot\alpha_w)} \cdot \frac{2}{k_c} \cdot \frac{\Delta\rho \cdot g}{\rho_o} \cdot \frac{dh_w}{d\alpha_w} \tag{26}$$

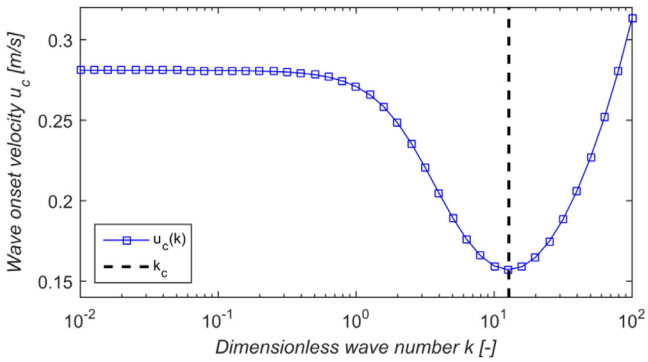

Fig. 12. Example of how the wave onset velocity u_c varies with the dimensionless wave number k.

4.5. Modelling of wavy oil/water flows

We now have an expression for estimating the wave onset velocity u_c (Eq. (26)), and we may presume that waves will appear as soon as the oil/water slip velocity exceeds that value. This means that the interfacial friction coefficient will at that point depart from the smooth model given by Eq. (20) and become larger. A reasonable guess for how the interfacial friction coefficient could be formulated is:

$$f_i = f_{i,smooth}\left[1 + C \cdot \max\left(\frac{\Delta u - u_c}{u_c}, 0\right)\right] \tag{27}$$

Here, C could either be a constant or some function of the flow parameters. This particular formulation provides a transition from smooth to wavy flow that is consistent with the VKH analysis above. Furthermore, this model assumes that the interfacial friction coefficient increases with the "distance" from the onset, where the distance is represented by the dimensionless group $\Delta u/u_c$. We refer to the second term inside the parenthesis in Eq. (27) as the "wave factor". We use this term because it is a factor that describes how the friction factor departs from the smooth model in the presence of interfacial waves.

In Fig. 13 we have plotted the experimentally obtained wave factor against $\Delta u/u_c$-1. Notice that the parameter selected for the x-axis is the same expression that we have used in the wave factor in Eq. (27). The wave factors line up very well for all the data

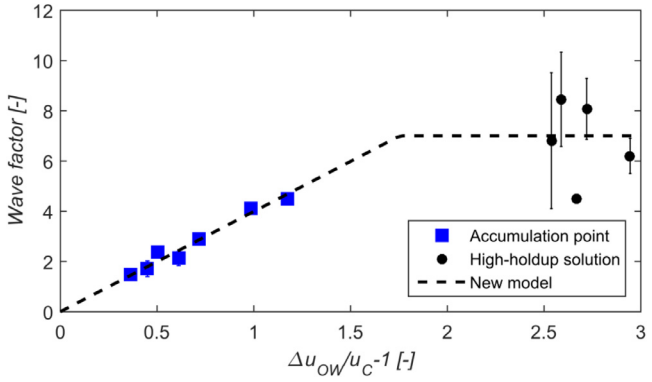

Fig. 13. Wave factor plotted versus $\Delta u/u_c$-1. The black dashed line indicates the shape of the new model.

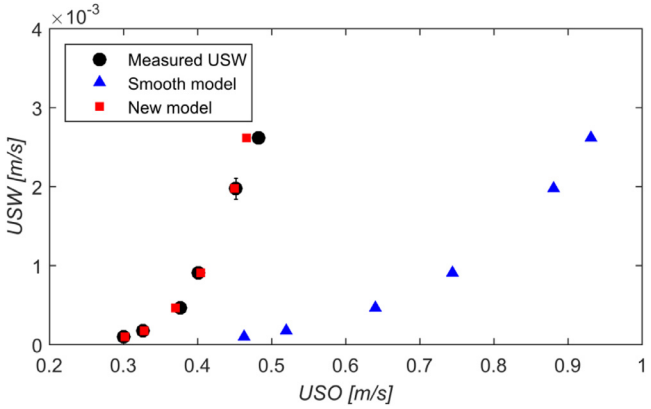

Fig. 14. Experimental and simulated outlet water rate plotted against *USO* for the screening experiments. The red squares represent the results obtained with Eq. (28).

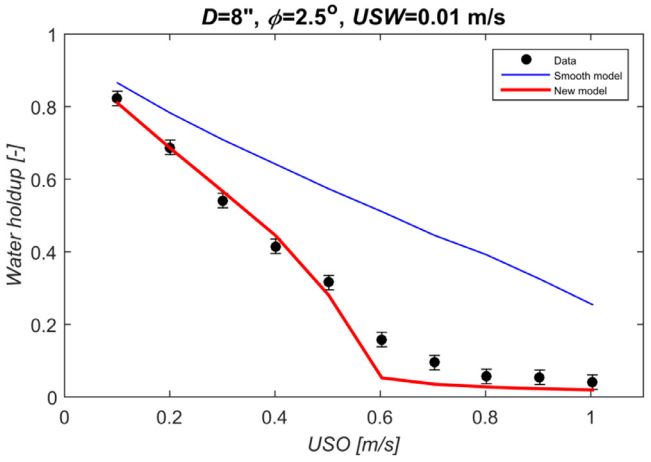

Fig. 15. Experimental and simulated water fraction plotted against *USO* for the steady-state experiments. The red squares represent the results obtained with Eq. (28).

points calculated from the screening experiments, and the black dashed line that we have drawn through these points intersects the origin. The slope of this line corresponds to the coefficient C in Eq. (27), and the data suggests that a value of C=4.0 gives the best fit. This result is encouraging, because this means that the wave factor approaches zero when the slip velocity approaches the wave onset velocity u_c, which is what is supposed to happen. This lends credence to the analysis used to determine u_c, and it suggests that the simplifications made in that analysis are reasonable.

It is worth noting that we first attempted using Inviscid Kelvin-Helmholtz analysis instead of Viscous Kelvin-Helmholtz analysis, but then the line through the data points did not intersect the origin. Consequently, including the effect of viscosity on the normal stresses seems important in this analysis.

We observe that data points at higher slip velocities (the black circles, which are from the steady-state experiments with high holdup) do not collapse on the same line. Indeed, given the scatter in those points it is not possible to draw a line that intersects all of them, but the average value for this cluster of points is around 7.0. The reason that these data points do not line up so well is not clear, but the most likely explanation is that the interfacial shear stress is a more complex matter at high water holdups. Indeed, the interfacial waves at high water holdups have large amplitudes and may depend on other factors than what we have assumed in our model. Also, as we have pointed out earlier, the procedure used to calculate those points has some significant weaknesses. In any case, it seems that a reasonable extension of the model described by Eq. (27) may be to introduce a plateau, as the black dashed line shown in Fig. 13 indicates. The final version of the model is thus:

$$f_i = f_{i,smooth}\left[1 + \min\left[4.0 \cdot \max\left(\frac{\Delta u - u_c}{u_c}, 0\right), 7.0\right]\right] \tag{28}$$

4.6. Model verification

In this section we show the results obtained with the new model proposed in the previous section (Eq. (28)). The data shown in this section is the same data that we used to derive the model, so we perform this exercise only to verify that our analysis was carried out correctly.

In Fig. 14 we show the outlet water rate plotted against *USO* for the screening experiments. The black circles are the measured values, while the blue triangles and red squares are predictions using the smooth interface model and Eq. (28), respectively. We find that the new model matches the measured values well, certainly much better than the smooth interface model.

In Fig. 15 we show the results from the steady-state experiments, where *USO* was varied from 0.1 to 1 m/s, using a fixed superficial water velocity of *USW*=0.01 m/s. The black circles represent the measured values while the thin blue line and thick red line are the predictions using the smooth interface model and Eq. (28), respectively. Again, we see that the new model clearly outperforms the smooth interface model. The new model does however slightly under-predict the water fraction for the highest oil rates. The reason for this is unclear, but it could be due to weaknesses in the applied wall friction model.

In Fig. 16 we have combined the results shown in Fig. 14 and Fig. 15 to illustrate more clearly what the screening experiments actually represent. In each of the graphs in this figure we have plotted the water fraction versus the superficial oil velocity for different values of *USW* (which is indicated as text in each graph). Most of the data points shown in these graphs are actually taken from the steady-state experiments conducted with *USW*=0.01 m/s, but we have taken the liberty to include them in these graphs because the water holdup on the high-holdup branch is known to be virtually independent of the water rate at such small superficial water velocities. This is something that we have observed in the experiments, and the model results that we have included in these graphs confirm this result. In other words, if we had performed steady-state experiments at all the designated water rates, the prevailing water fractions in the high-holdup-region would

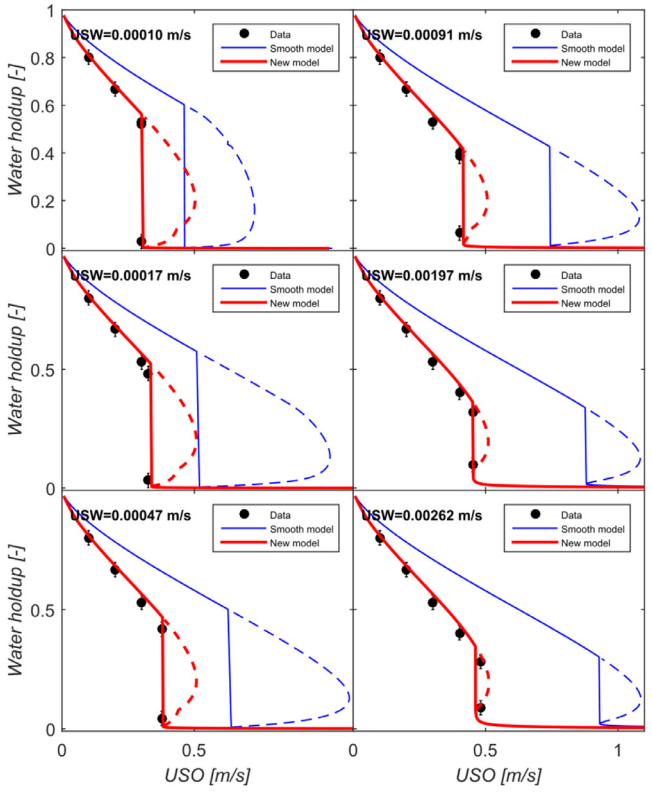

Fig. 16. Water fraction plotted against *USO* for various *USW*-values. The thick red lines represent the results obtained with Eq. (28).

presumably have been indistinguishable from the values obtained at USW=0.01 m/s. The physical rationale for this assumption is that at these low water rates ($USW \leq 0.01$ m/s) the water velocity $u_w = USW/\alpha_w$ is necessarily very low when the water holdup α_w is high, and may thus be reasonably approximated by a value of zero in the momentum equations. The prevailing momentum balance, and by extension the water holdup, is thus virtually independent of the value of USW in this situation.

The last two (right-most) data points in each graph in Fig. 16 are taken from the screening experiments, where the high value is the measured water fraction upstream of the water front, and the low values is the measured water fraction downstream of the water front. These water fraction data points from the screening experiments were obtained by converting the water heights measured by the static gamma densitometers into volume fractions by assuming a flat interface. As illustrated in Fig. 8, these two water fraction values represent the high/low solutions at the accumulation point. We have included no datapoints beyond the accumulation point because the data points obtained with USW=0.01 m/s would generally not be comparable to values obtained at lower USW on the low-holdup-solution branch.

The thin blue lines are predictions using the smooth interface model, while the thick red lines are predictions obtained using Eq. (28). We have elected to show all three water holdup solutions in these graphs, where the dashed part of the curves represents the solutions that are not relevant for these experiments. As expected, we observe that the predictions obtained with the new model is in good agreement with the experimental values, while the smooth interface model is clearly unsuitable for predicting these types of scenarios.

5. Conclusions

In this paper we have described a set of oil-water experiments conducted at the SINTEF Multiphase Laboratory in a 94 meter long 8" pipe. The experiments were specially designed to measure the critical conditions for water accumulation in oil/water flows. The experiments were performed at a pipe inclination of 2.5 degrees using Exxsol D60 as the oil phase and tap water as the aqueous phase.

The data showed that the critical oil velocity for water accumulation increases with increasing water flow rate. The data analysis also showed that a "smooth" interfacial friction factor is unsuitable for predicting the onset of water accumulation, and that the effect of interfacial waves must be incorporated to model such scenarios. We found that the onset of interfacial waves is accurately predicted by the Viscous Kelvin-Helmholtz theory described by Funada & Joseph (Funada and Joseph, 2001).

Based on this data analysis, a new model for oil/water interfacial shear stress was developed, and this new model significantly improves the agreement with the measurements compared to the smooth friction factor. A slightly modified version of this model has since been implemented in the transient multiphase flow simulator LedaFlow ("LedaFlow, " Kongsberg Digital AS, 2020).

Declaration of Competing Interest

There is no conflict of interest associated with this manuscript.

Acknowledgements

The authors would like to thank the technical and scientific personnel at the SINTEF Multiphase Laboratory for their considerable efforts during the experimental campaigns. We would also like to express our appreciation to LedaFlow Technologies DA (owned by SINTEF, Kongsberg Digital, Total and ConocoPhillips) and the Norwegian Research council (grant number 281881), for financing the model development described here, as well as this publication.

References

Barnea, D., Taitel, Y., 1992. Structural and interfacial stability of multiple solutions for stratified flow. Int J Multiphase Flow 18 (6), 821–830.
Bluemink, E. "Fairbanks Daily News-Miner," 3 Jan 2010. [Online]. Available: http://www.newsminer.com/news/alaska_news/less-oil-may-spell-more-problems-for-trans-alaska-pipeline/article_3cecf9ac-8076-53c0-8c4a-9fc00acf2e61.html. [Accessed 24 June 2020].
Brauner, N., Maron, D.M., Rovinsky, J., 1998. A two-fluid model for stratified flows with curved interfaces. International Journal of Multiphase Flow 24, 975–1004.
Funada, T., Joseph, D., 2001. Viscous potential flow analysis of Kelvin–Helmholtz instability in a channel. Journal of Fluid Mechanics 445, 263–283.
Johansson, P.S., Pettersen, B.H., Djoric, B., 2013. Ramp-up and Rampdown of Low Liquid Loading Gas-Condensates Flowlines. International Conference on Multiphase Flow.
Hall, A., Hewitt, G., 1993. Application of two-fluid analysis to laminar stratified oil-water flows. Int. J. Multiphase Flow 19, 711–717.
Håland, S., 1983. Simple and Explicit Formulas for the Friction Factor in Turbulent Flow. Journal of Fluids Engineering (ASME) 105 (1), 89–90.
Kjølaas, J., Holm, H., 2016. Improvement of LedaFlow for low liquid loading conditions. 10th North American Conference on Multiphase Technology *ISBN 9781855981553*.
Kjølaas, J., Unander, T.E., Wolden, M., Johansson, P.S., Holm, H., 2015. Experiments for low liquid loading with liquid holdup discontinuities in two- and three-phase flows. 17th Multiphase Production Technology Conference, ISBN 9781855981478.
Landman, M., 1991. Non-unique holdup and pressure drop in simulations of two-phase stratified inclined pipe flow. Int J Multiphase Flow 17 (3), 377–394.
"LedaFlow, " Kongsberg Digital AS, [Online]. Available: http://www.ledaflow.com/. [Accessed 24 June 2020].
Magill, B. "Popular mechanics," 1 February 2012. [Online]. Available: https://www.popularmechanics.com/science/energy/a7480/how-much-life-is-left-in-the-trans-alaska-pipeline/. [Accessed 24 June 2020].
Taitel, Y., Barnea, D., Brill, J., 1995. Stratified three phase flow in pipes. International Journal of Multiphase Flow 21 (1), 53–60.

"Trans Alaska Pipeline System - The facts, " Alyaska Pipeline Service Company, 2019. [Online]. Available: https://www.alyeska-pipe.com/TAPS/PipelineFacts. [Accessed 24 June 2020].
Ullmann, A., Zamir, M., Gat, S., Brauner, N., 2003. Multi-holdups in co-current stratified flow in inclined tubes. International Journal of Multiphase Flow 29, 1565–1581.
Valle, A., 2000. Three Phase Gas-oil-water Pipe Flow. University of London, London.
Valle, A., Kvandal, H., 1995. Pressure drop and Dispersion Characteristics of Separated Oil-Water Flows. Int. Symp. on Two-Phase Flow Modelling and Experimentation.
Zaghloul, J., Adewumi, M., Ityokumbul, M.T., 2008. Hydrodynamic Modeling of Three-Phase Flow in Production and Gathering Pipelines. J. Energy Resour. Technol 130 (4), 043004 (4)(8 pages).